ACS APPLIED MATERIALS & INTERFACES

www.acsami.org

Research Article

Antifouling Electrochemical Biosensor Based on Conductive Hydrogel of DNA Scaffold for Ultrasensitive Detection of ATP

Xiaoyan He,* Nan Sun, Hui Jia, Miaomiao Hou, Zheping Tan, and Xiaoquan Lu*

Cite This: *ACS Appl. Mater. Interfaces* 2022, 14, 40624−40632

Read Online

ACCESS | Metrics & More | Article Recommendations | Supporting Information

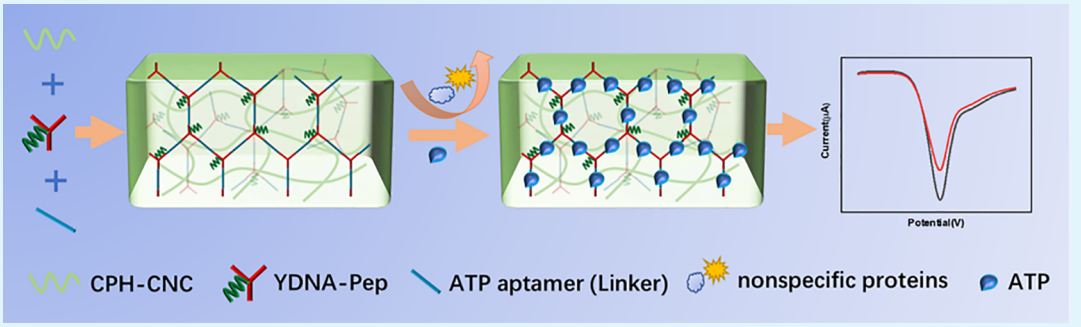

ABSTRACT: As an energy supplier, ATP plays an important role in various life activities, and there is an urgent need to develop an effective means of detecting ATP. However, the traditional sensors face serious nonspecific adsorption. In this work, an antifouling electrochemical biosensor based on the interpenetrating network of Y-DNA scaffold and polyaniline hydrogel was designed for ATP detection. The polyaniline hydrogel was conducive to the transport of electrons and ions, the structure of Y-DNA cross-linked by ATP aptamers in the polyaniline hydrogel achieved the effect of signal amplification. Super hydrophilic cellulose nanocrystals (CNCs) and zwitterion polypeptide sequence (Pep) were doped to play a synergistic antifouling effect. The hydrogel sensor we have built has a wide linear range of 0.1 pM−1 μM for ATP detection and a low detection limit of 0.025 pM (S/N = 3). For ATP detection in actual serum samples, the recovery of this sensor was 99.5%−106%, and the relative standard deviation was 0.4%−2.88%. It is proven that the sensor has good ATP detection performance, and it will provide a certain reference value for the detection of other biological small molecules.

KEYWORDS: *polyaniline, DNA, hydrogel, nonspecific adsorption, adenosine triphosphate*

INTRODUCTION

Chemical nerve substances play a very important role in brain function, and the detection of their relative content in the human body to prevent various related diseases has aroused the strong interest of researchers.[1] Adenosine triphosphate (ATP) is a multifunctional nucleotide that is considered to be the main energy currency in biology; it plays an important role in regulating cell metabolism, signal transduction, and other biological processes.[2−4] As a biomarker of many clinical diseases such as Parkinson's disease, Alzheimer's disease, and hypoglycemia, the detection of ATP counted for much, and it is urgent to develop an effective method of ATP detection.[5−7]

At present, electrochemistry,[8] electrochemiluminescence,[9] high-performance liquid chromatography,[10] mass spectrometry (MS),[11] fluorescence,[12] and other methods have been used for the detection of ATP. Among them, an electrochemical sensor has attracted more and more attention because of its low test cost, simple instrument operation, fast test data, and high sensitivity.[13] Although these methods have been used for ATP sensing, due to the complexity of the detected media and the low level of ATP content, the detection accuracy of electrochemical biosensors is reduced due to biocontamination. Therefore, the selective and sensitive detection of ATP still remains a challenge; it is necessary to construct an antipollution sensing interface to improve the highly selective detection of ATP. Due to the complexity of the detection environment, many interferences will affect the detection performance of sensors. Facing this challenge, a lot of work has been done in this area recently. For example, Tang's[14,15] research group detected CTnI protein using liposome-embedded $Cu_{2-x}Ag_xS$ nanoparticle-mediated photothermal immunoassay, which achieved good selectivity for target objects. In the past decades, people have explored the construction of various antifouling interfaces, including physical, chemical, and biological antifouling.[16] Physical antifouling is

Received: June 6, 2022
Accepted: August 24, 2022
Published: September 1, 2022

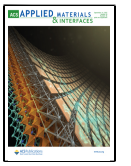

Table 1. Sequences of Oligonucleotides Used in this Work

oligonucleotide	sequence (5′ to 3′)
Y_1	COOH-CGATTGACTCTCGCTGTCCTAACCATGACCGTCG
Y_2	CGATTGACTCTCCGACGGTCATGTACTAGATCAG
Y_3	CGATTGACTCTCCTGATCTAGTAGTTAGGACAGC
linker	GAGAGTCAATCGACCTGGGGGAGTATTGCGGAGGAAGAGAGTCAATCG

mainly based on the design of hierarchical porous structure to reduce the adhesion of biological pollutants due to the structural limitation of the interface.[17,18] Chemical antifouling is mainly achieved by introducing antifouling materials, such as polyethylene glycol,[19] amphoteric ion betaine sulfonate,[20] bovine serum albumin,[21] cellulose nanocrystals,[22] and peptides.[23−25] However, the synthesis and assembly of these materials on the sensor surface is complex, and most of the antipollution materials have poor electrical conductivity, resulting in high impedance on the electrode surface, which reduces the sensitivity of the biosensors. Therefore, introducing conductive polymers to modify the electrode together with antipollution materials has become the research hotspot in the construction of biosensors.

On the basis of the conducting polymers such as polythiophene, polyaniline, and polypyrrole, conductive hydrogels combine the advantages of organic conductors and hydrogels, having the advantages of good biocompatibility, mechanical properties, hydrophilicity, conductivity, 3D nanostructures, and large specific surface area.[26−28] In many of the conductive polymer hydrogel, polyaniline-based hydrogels have attracted extensive attention because of their excellent mechanical properties, no labels, high electronic conductivity, redox reversibility, and good biocompatibility.[29,30] Furthermore, polyaniline hydrogels have antifouling properties due to their high specific surface area and a variety of pore structures.

In this work, the negatively charged DNA scaffold (DNA) and the positively charged skeleton of conductive polyaniline hydrogel (CPH) are combined by electrostatic, $\pi-\pi$ hydrogen bond, and physical entanglement to detect ATP. ATP aptamers and polypeptide-modified YDNA scaffolds are connected to each other by base complementary pairings (ATP aptamers as linkers), forming DNA networks[31−33] in situ at CPH. On the contrary, due to the formation of a hydrogel, the aptamer could spread all over the hydrogel network in a three-dimensional way, increasing the active sites of target substance and improving the detection sensitivity. The super hydrophilic cellulose nanocrystals (CNCs) and zwitterionic polypeptide sequences (Pep) were semi-interpenetrating in the hydrogel as antipollution materials to realize multiple antifouling. The results showed that the constructed CPH-based aptamer antifouling sensor has a wide detection range and a low limit for ATP detection, which can provide a certain reference value for the detection of other biological small molecules.

2. EXPERIMENTAL SECTION

2.1. Chemicals and Materials. Adenosine triphosphate (ATP) was supplied from Energy Chemical (Shanghai, China). Ammonium persulfate was purchased from Yantai Shuangshuang Chemical Co., Ltd. Guanosine triphosphate (GTP), adenosine diphosphate (ADP), 3-aminobenzene boric acid (ABA), *N*-hydroxysulfosuccinimide (NHS), *N*,*N*,*N*′,*N*′-tetramethylethylenediamine, and *N*-(3-(dimethylamino)-propyl)-*N*′-ethylcarbodiimide hydrochloride (EDC) were purchased from Aladdin Reagents (Shanghai, China). Uridine triphosphate (UTP) was purchased from Macklin (Shanghai, China). Cellulose nanocrystals were purchased from Kunshan Hopu Fiber Technology Co., Ltd. Bovine serum albumin (BSA), β-lactoglobulin (β-Lg), and lipoprotein lipase (LPL) was purchased from the Shanghai Yuanye Biological Technology Co., Ltd. Aniline, ascorbic acid (AA), L-glycine (Gly), and tris(hydroxymethyl) methyl aminomethane (Tris) were purchased from Shanghai Zhongqin Chemical Reagent Co., Ltd. Sodium dihydrogen phosphate, disodium hydrogen phosphate, and ethylenediamine tetraacetic acid disodium salt (EDTA) were purchased from Tianjin Damao Chemical Reagent Factory. Potassium ferricyanide and poly(vinyl alcohol) (1750) were purchased from Tianjin Kaixin Chemical Industry Co., Ltd. Peptides (EKEKEKEK) were synthesized by Bankpeptide Biological Technology Co., Ltd (Hefei, China). All of the sequences of oligonucleotides used in this work are given in Table 1, and all other chemicals used in this paper were of analytical grade.

2.2. Apparatus. All electrochemical characterization was performed by an electrochemical workstation (CHI660E, Shanghai Chenhua Instrument Co. Ltd, China) with a three-electrode system. The working electrode is a glassy carbon electrode, the reference electrode is a saturated calomel electrode, and the counter electrode is a platinum wire electrode. Morphological measurements were performed using a JEOL JSM-6701FGSM-5600LV scanning electron microscope (SEM) (JEOL). Fourier transform infrared (FT-IR) spectra were recorded by a model FTS-23000 (Digilab) spectrometer.

2.3. Preparation of DNA Network (DNA) and YDNA Scaffold−Polypeptide (YDNA−Pep). For the preparation of a DNA hydrogel network: single stranded DNA Y1, Y2, and Y3 were mixed in equal mole ratio and lyophilized to obtain a white solid. Then, PBS solution was added, and the sample was heated to 95 °C for 5 min and slowly cooled to room temperature to obtain the Y-scaffold solution. The linker solution consisting of aptamer was prepared using a similar method. The two solutions were then evenly mixed at room temperature to form a DNA network. For the preparation of the YDNA scaffold−polypeptide solution: NHS (20 μM) and EDC (20 μM) were added to a solution of 10 μM YDNA scaffold for incubation for 1 h to activate the carboxyl group. Then 10 μM polypeptide solution was added to the above step solution, and the mixture was incubated for 12 h. The YDNA scaffold was coupled to the polypeptide sequence EKEKEKEK by an amide bond. We labeled it as YDNA−Pep.

2.4. Preparation of CPH−CNC Hydrogels. Conductive hydrogels were prepared by referring to the previous literature.[34] Aniline (1.5 mmol) and 0.105 mmol of aminobenzenboric acid were added to a mixed solution of 6 M HCl and H_2O. Next, 0.05 mg/mL cellulose nanocrystalline dispersion was added, and the above solution was placed in 3 mL of a poly(vinyl alcohol) (10 wt %) solution to form a homogeneous mixed solution. The mixed solution was labeled as liquid A. Two millimoles of ammonium persulfate was dissolved in deionized water to form liquid B. Then, the solutions A and B were cooled to 0 °C in an ice water bath. Solution A was added to solution B, and the mixture was reacted for 6 h to form a polyaniline conductive hydrogel, which was soaked in water to remove the unreacted impurities for later use. Porous CPH−CNC conductive hydrogel was obtained (Figure S1).

2.5. Fabrication of the Antifouling Electrochemical Sensor. First, 3 μL of the CPH precursor solution was dropped onto the surface of a clean glassy carbon electrode to form a conductive hydrogel layer. Then, it was soaked in deionized water for 30 min to remove the unreacted ingredients. The cyclic voltammetry (CV) technique was used to activate the electrode modified with CPH−CNC in 0.2 M PB aqueous solution, with a scanning range from −0.6 to +0.4 V, and the scan rate was 0.05 V/s. Subsequently, 6 μL of the YDNA− Pep was dropped on the CPH−CNC/GCE for 2 h. After that, 3 μL of the

https://doi.org/10.1021/acsami.2c10081
ACS Appl. Mater. Interfaces 2022, 14, 40624−40632

Scheme 1. Schematic Illustration of the Fabrication Process for the Novel Electrochemical Aptasensor

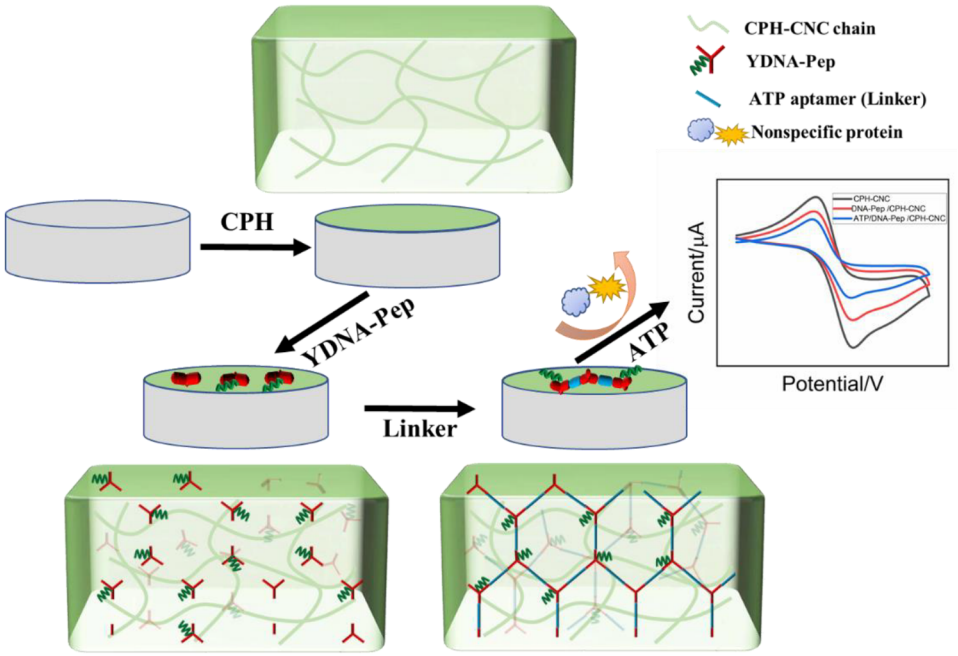

aptamer linker was dropped on the modified electrode and incubated for 1.5 h. Finally, the DNA−Pep/CPH−CNC/GCE was washed with deionized water to remove the unbound sequence. CV was used to evaluate the preparation process of the antipollution electrochemical sensor. The CV scanning range was −0.6 to +0.4 V and the scanning rate was 0.05 V/s. Differential peak pulse voltammetry (DPV) was also used to evaluate the electrochemical behavior of the sensor. DPV measurements were from −0.6 to +0.4 V with a pulse amplitude of 50 mV and a pulse period of 50 ms.

2.6. Antifouling Properties of Cellulose Nanocrystals (CNCs) and Zwitterionic Polypeptides (Pep) in Nonspecific Proteins and Serum. In order to evaluate the antifouling performance of the constructed sensor, three nonspecific proteins, BSA, β-Lg, and LPL, and serum were used for experiments. The DPV signal changes of CPH, CPH−CNC/GCE, and DNA−Pep/CPH−CNC/GCE modified electrodes before and after incubating in three kinds of nonspecific protein solutions (1.0 mg/mL) and serum were studied.

2.7. Antifouling Electrochemical Sensor for ATP Detection. Different concentrations of ATP were added to the surface of DNA−Pep/CPH−CNC/GCE to incubate for 1.5 h. Then, DPV was performed to detect ATP in the PB solution (pH = 7.4) containing 0.2 M Na_2HPO_4.

2.8. ATP Content in Serum Samples was Detected. In order to evaluate the detection performance of the antifouling biosensor in actual samples, we prepared serum samples to complete the exploration. The serum was treated according to the previous report,[35] and the DPV method was used to carry out the standard recovery experiment at room temperature.

3. RESULTS AND DISCUSSION

3.1. Mechanism of Electrochemical Antifouling Detection of ATP. In this work, the outline of the antifouling electrochemical sensor developed is shown in Scheme 1. CPH combines the advantages of organic conductors and hydrogels. First, the glassy carbon electrode was coated by the CPH−CNC, which was activated by cyclic voltammetry. Then, the YDNA−Pep was drip-coated and modified on the electrode. ATP aptamer with complementary base sequences linking to the YDNA scaffold aimed to connect each YDNA scaffold to form a YDNA network. This network can be combined with CPH−CNC by hydrogen bonding, electrostatic effect, and physical winding to form a double network hydrogel. Due to the formation of the DNA network, ATP aptamer spreaded all over the entire surface of the hydrogel network, which hoped to increase the target sites of ATP and realize the ultrasensitive detection of ATP. Polyaniline hydrogels provide high electrical conductivity; when the target ATP is present, it specifically binds to the ATP aptamer in the hydrogel network, and as an inactive substance, ATP hinders the transmission of electrons, leading to the reduction of the redox peak and resulting in a significant reduction of DPV current signal. Moreover, the decrease of the electrochemical signal is related to the increase of ATP concentration. In order to prevent nonspecific adsorption in complex media, super hydrophilic CNC and Pep sequences are introduced, which combine with water molecules to form a dense hydration membrane to prevent nonspecific adsorption of hydrophobic substances such as proteins and used for antifouling detection of ATP.

3.2. Characterization of Synthesized CPH, CPH−CNC, and DNA−Pep/CPH−CNC hydrogel. To confirm the successful polymerization steps, the FTIR of CPH, CPH−CNC, DNA−Pep/CPH−CNC, and other related monomers are studied in Figure S2. In Figure S2A, curve a is the FTIR curve of poly(vinyl alcohol); the peaks at 3433, 2918, and 1049 cm^{-1} are the stretching vibration of O—H, C—H, and C—O of PVA, respectively.[36] The absorption peak at 3230 cm^{-1} is attributed to the stretching vibration of N—H in an amino group of 3-aminobenzene boric acid (curve b). In the infrared data figure of monomer aniline (curve d), the absorption peaks at 3356 cm^{-1} belong to the stretching vibration peak of N—H in an amino group. In the spectrum of the synthesized polyaniline−poly(vinyl alcohol) conductive hydrogel (curve c), two characteristic peaks at 1633 and 1402 cm^{-1} correspond to the stretching vibration of quinone ring and benzene ring.[37] The N—H stretching vibration peaks of the amino group in aniline and 3-aminobenboric acid disappeared in the conductive hydrogel compared with the monomer 3-aminobenboric acid

https://doi.org/10.1021/acsami.2c10081
ACS Appl. Mater. Interfaces 2022, 14, 40624−40632

and aniline, indicating that the polymerization of aniline and 3-aminobenboric acid occurred through the amino group. After introducing CNC into CPH, as shown in Figure S2B, compared with CPH (Figure S2B, a), the —OH peak at 3439 cm^{-1} increased (Figure S2B, b), indicating that CNC was successfully introduced as a component of CPH.[38] After modification of the polypeptide in CPH (Figure S2B, c), the peak at 1635 cm^{-1} is attributed to the stretching vibration of C═O bond in the amide bond of the polypeptide sequence. The peak at 617 cm^{-1} is attributed to the flexural vibration of a C═O bond in the amide bond, which proves that the polypeptide has been successfully introduced into CPH−CNC.

To prove the structures of the CPH, CPH−CNC and DNA−Pep/CPH−CNC, the figure of the SEM is exhibited. As shown in Figure 1A, we can observe the rich porous structure of

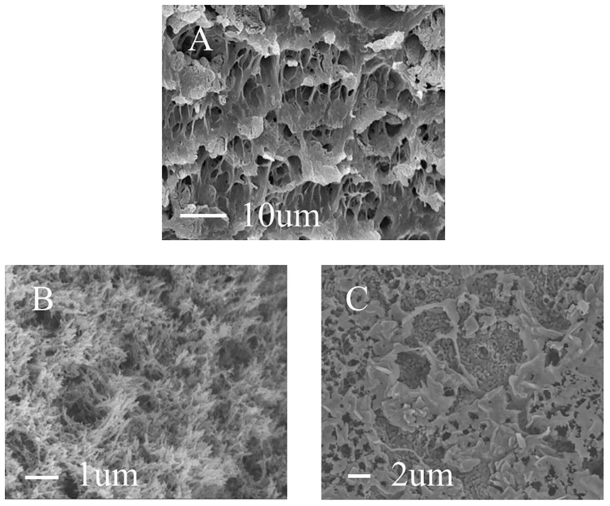

Figure 1. SEM images of (A) CPH, (B) CPH−CNC, and (C) DNA−Pep/CPH−CNC.

polyaniline hydrogel, which helped with the transmission of the electron and biomolecular enrichment. After modification of the CNC, it can be seen from Figure 1B that CNC is evenly distributed in the conductive hydrogel without affecting the porous structure of the hydrogel, which is used as an antifouling material for the construction of sensors. After the YDNA scaffold with modified polypeptides was dripped onto the CPH−CNC hydrogel (Figure 1C), a different structure is shown, imply that the DNA scaffold was doped into it for the subsequent target specificity detection.

3.3. Antifouling Capability of Electrochemical Sensor. In order to evaluate the antifouling performance of the interface of hydrogel sensor based on DNA and polyaniline interpenetration network, three monoproteins (BSA, β -Lg, and LPL) were prepared in a PB solution (0.2M, pH = 7.4) with a concentration of 1.0 mg/mL. The DPV method was used to test the antipollution performance of the sensor in these three complex media. The DPV current signals of electrodes, CPH, CPH−CNC, and DNA-Pep/CPH−CNC hydrogels were compared before and after incubation in three protein solutions. As shown in Figure 2, the signal changes of the CPH-modified electrode were relatively significant before and after incubation (the first column). After incubation, the DPV current responses of the CPH-modified electrode in BSA, β-Lg, and LPL were 23%, 13.2%, and 12.7% of the original value, respectively. This is mainly attributed to the porous structure of the polyaniline hydrogel; the limitations lead to certain physical antifouling performance. The porous structure allows small molecules to pass through while restricting the entry of large molecules such as proteins, which acts as a filter preventing nonspecific adsorption of the sensor. It can be concluded that only part of the protein adhered to the electrode surface, which obstructed electron transfer and caused the reduction of electrochemical signal. As shown in the second column of Figure 2, when the CNC was introduced further, the signal changes of DPV were significantly reduced. After the CPH−CNC hydrogels were cultured in BSA, β-Lg, and LPL, the DPV current changes were 4.5%, 6.9%, and 5.8% of the original value, respectively. This is attributed to the super hydrophilic properties of polyhydroxyl functional groups on the cellulose nanocrystals; a dense hydration layer could be formed, which acts as a strong physical barrier and prevents the diffusion and infiltration of proteins on the substrate surface. As shown in the third column of Figure 2, the antipollution effect of the DNA-Pep/CPH−CNC hydrogels modified electrode was significantly improved by adding the amphoteric ion polypeptide sequence on the basis of the above materials. After incubation in BSA, β -Lg, and LPL, the DPV current response was 2.5%, 1.7%, and 1.5% of the original value, respectively. This may be due to the strong binding effect between the amphoterionic polypeptide sequence and water molecules, which could form a hydration layer to prevent nonspecific adsorption. Therefore, cellulose nanocrystals and polypeptide sequences all have strong interactions with water molecules, forming a dense hydration film. The synergistic antifouling effect of the two and the physical antifouling effect of porous hydrogel itself are combined to greatly improve the protein avoidance performance of the sensor. As a result, the sensor of the DNA−Pep/CPH−CNC hydrogels proved to have excellent antifouling performance in complex media.

In addition, the DPV method was used to evaluate the antifouling properties of three hydrogel modified electrodes of CPH, CPH−CNC hydrogels, and DNA−Pep/CPH−CNC hydrogels in serum. Figure 3 shows that the current signal of the CPH modified electrode changes greatly after incubation in serum, indicating that the physical antifouling performance of the porous electrode is not obvious. After the introduction of hydrophilic CNC, the change of DPV signal in serum decreased, indicating that super hydrophilic cellulose nanocrystals have a certain antifouling performance. After introducing DNA−Pep into the hydrogel, the signal value before and after incubation in serum was almost unchanged. It shows that the synergistic antifouling effect of physics and chemistry is obvious. This result is consistent with the signal in three different protein solutions, indicating that the antifouling material has a better synergistic antifouling effect.

3.4. Electrochemical Characterization of Different Electrodes. CV and DPV were used to characterize the electrochemical behavior of different modified electrodes. In the CV curve, as shown in Figure 4A (CPH−CNC hydrogel modified glassy carbon electrode), due to the redox action of PANI, we can clearly see that the CV curve has an obvious redox peak and a large current signal (curve a). When it was modified by the DNA network containing the polypeptide sequence (curve b), the current signal was significantly reduced, which is attributed to the electron transferring blocking of the polypeptide sequence EKEKEKEK and the DNA network. In the presence of ATP (Curve c), the current signal is further reduced, indicating that ATP specifically binds to aptamers in the hydrogel network. ATP is an inactive substance that hinders

https://doi.org/10.1021/acsami.2c10081
ACS Appl. Mater. Interfaces 2022, 14, 40624−40632

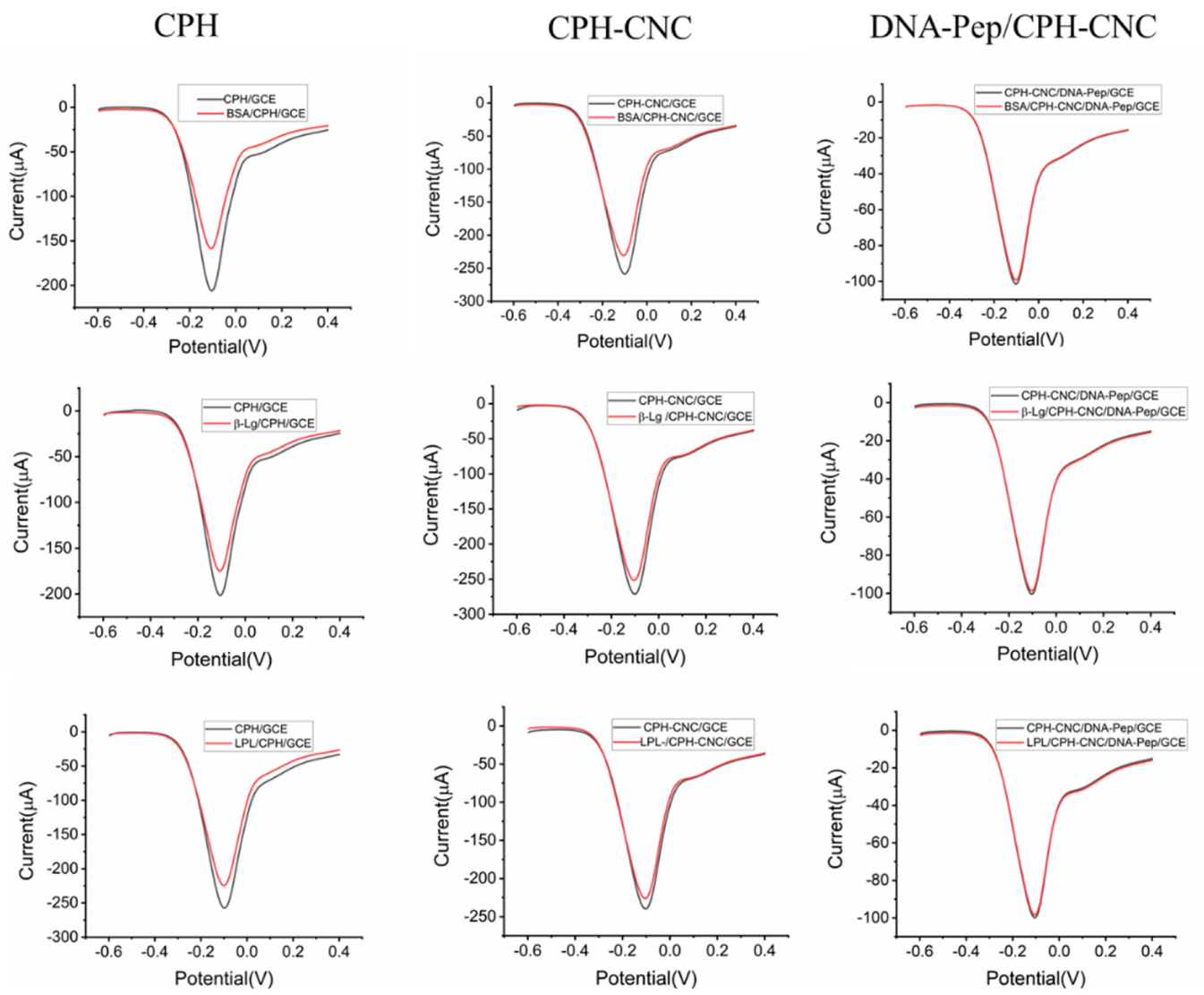

Figure 2. DPV current changes of CPH, CPH/CNC, and DNA−Pep/CPH−CNC modified electrodes before (black line) and after (red line) incubation in three protein solutions (1, BSA; 2, *β*-Lg; and 3, LPL, 1.0 mg/mL each).

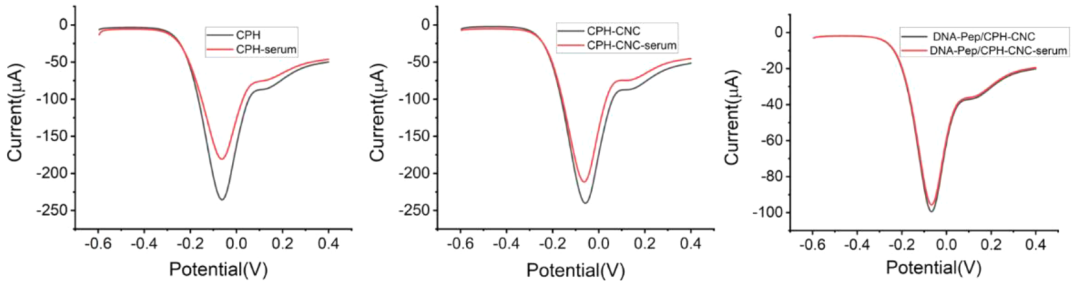

Figure 3. DPV current changes of CPH, CPH−CNC, and DNA−Pep/CPH−CNC modified electrodes before (black line) and after (red line) incubation in serum.

the transmission of electrons, leading to the reduction of the redox peak. DPV curve (Figure S3) was used to characterize the current signal changes of the sensor with (red curve) and without (black curve) ATP aptamer in the presence of the target ATP. As can be seen from Figure S3, when aptamers are introduced into the sensor, there is a significant change in the current signal before (a) and after (b) ATP incubation, and the current signal change of the sensor without the aptamer is not obvious, which proves that the system has a recognition effect on ATP rather than an adsorption effect. In addition, DPV detection was also performed in PB solution (0.2 M, pH = 7.4) when the scanning range was −0.6 V to +0.4 V. As shown in Figure 4B, the results are consistent with those obtained by cyclic voltammetry. Therefore, under the antifouling environment provided by the composite hydrogels, specific binding between target and aptamer occurred, and the enrichment of the

https://doi.org/10.1021/acsami.2c10081
ACS Appl. Mater. Interfaces 2022, 14, 40624−40632

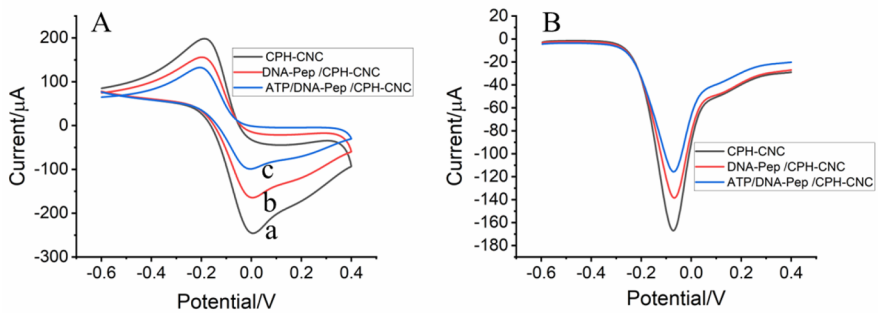

Figure 4. (A) CV curve and (B) DPV curve of the gradual electrode modification process.

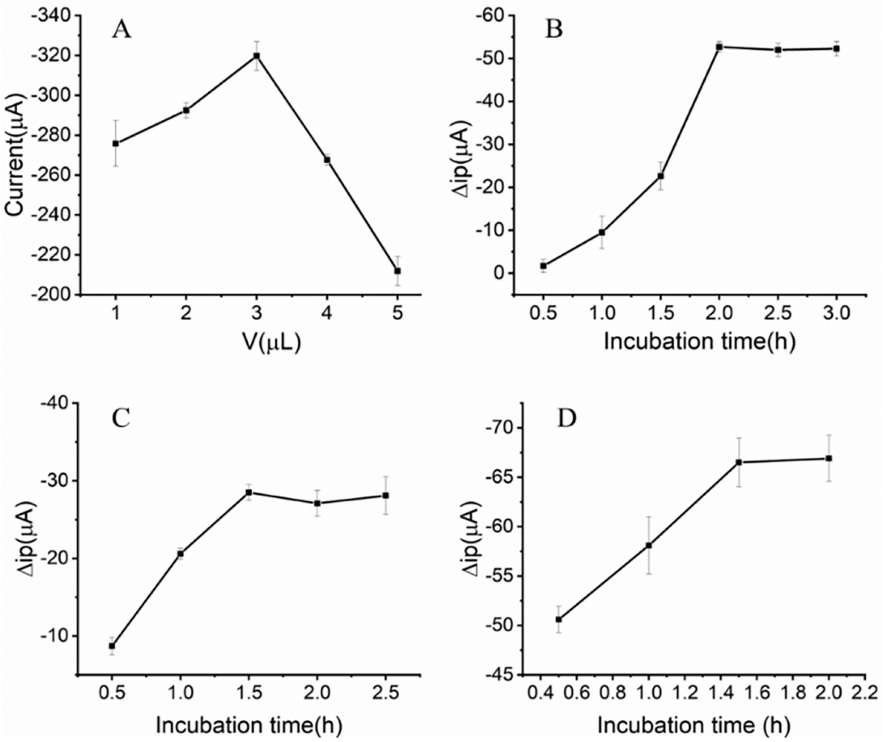

Figure 5. (A) Thickness optimization. (B) YDNA−Pep incubation time optimization. (C) APT aptamer incubation time optimization. (D) ATP incubation time optimization.

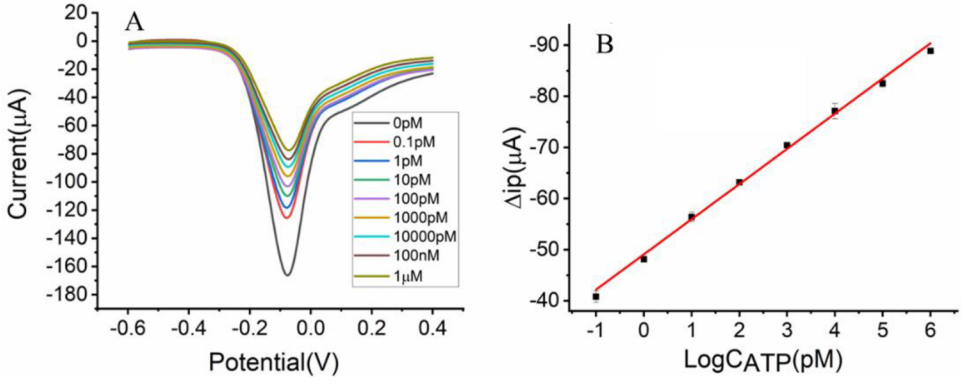

Figure 6. (A) DPVs of the electrochemical aptasensor after incubation with different concentrations of ATP. (B) Calibration curve of ATP for different ATP concentrations from 0.1 pM to 1 μM.

target by a hydrogel enabled the ultrasensitive detection of ATP. There is a good linear relationship between cyclic peak current and scanning rate, which indicates that this process is a surface-constrained process (Figure S4).

3.5. Optimization of Experimental Conditions. In order to obtain the optimal sensing performance, it is necessary to optimize the volume of conductive hydrogel and incubation time of YDNA scaffold, ATP aptamer, and ATP. First, DPV was

https://doi.org/10.1021/acsami.2c10081
ACS Appl. Mater. Interfaces 2022, 14, 40624−40632

used to optimize the volume of CPH. It can be seen from Figure 5A that the optimal volume is 3 uL. On this basis, the DPV curve was used to optimize the incubation time of YDNA−Pep. The electrochemical response signal changed the most at a binding time of 2 h from Figure 5B; therefore, 2 h is the best time for the diffusion of YDNA−Pep in a conductive hydrogel. Under the optimal diffusion time of fixed YDNA−Pep, the best incubation time of the ATP aptamer was explored. As shown in Figure 5C, the optimal binding time of ATP aptamer and YDNA scaffold is 1.5 h. Finally, we optimized the incubation time of ATP, and it can be seen from Figure 5D that the optimal incubation time of ATP is 1.5 h.

3.6. Analysis Performance of the Proposed Antipollution ATP Sensor. DPV was used to detect different concentrations of ATP standard solutions in PB solution (0.2 M, pH 7.4), and the performance of the antipollution composite hydrogel sensor was evaluated according to the detection results. As can be seen from Figure 6A, within the range 0.1 pM to 1 μM, the DPV electrochemical signal decreased with the increase of ATP concentration. When the ATP specifically binds to DNA network linkers (ATP aptamers), it blocks the electron transport and causes a reduction in electrochemical signals. As shown in Figure 6B, the change value of DPV electrochemical signal (Δip (μA)) shows a good linear relationship with the log value of different ATP concentration (R^2 = 0.995). The regression equation is Δip (μA) = −6.88 LogC [ATP] − 49.07, and the minimum detection limit is 0.025 pM (S/N = 3). Compared with previous reports, the electrochemical aptamer sensor shows better performance (Table S1). The good test results obtained are mainly attributed to the following: (1) Polyaniline hydrogel has a high conductivity and porous structure, which is conducive to electron transmission. (2) Cellulose nanocrystals and peptides are antifouling materials, which reduced the nonspecific adsorption of sensors in complex media. (3) Through the interlocking network of the DNA hydrogel and the conductive hydrogel, the ATP aptamer spreads across the entire surface of the hydrogel network, which would increase the targeting site of ATP. (4) The porous network of hydrogel has enrichment effect and can realize signal amplification. (5) The poor conductivity of adenosine triphosphate: when it is specifically bound to the ATP aptamer, it will get into the surface and interior of the sensor, hindering the electron transmission at the interface of the electrochemical sensor and thereby showing a decrease in the electrochemical signal. (6) The antifouling performance of the electrochemical sensor also stems from the porous structure of the hydrogel. The porous structure allows small molecules to pass through while restricting the entry of large molecules, which acts as a filter, thus preventing nonspecific adsorption of the sensor. Given all of that, the antifouling composite hydrogel sensor can achieve ultrasensitive detection of ATP.

3.7. Specificity, Repeatabilityand Reproducibility of Antifouling Sensor. Because the detected environment is complex, many interferences will affect the detection performance of the sensor and it is necessary to test the specific performance of the constructed sensor for ATP detection. Various interfering molecules and proteins were selected, including AA, Gly, BSA, UTP, GTP, and ADP. The selectivity of the sensor was verified by the DPV method, and the experiment showed that the DPV signal did not change significantly in the higher concentration of the interference, while the DPV signal response was obvious in the presence of the target molecule ATP at a low concentration (Figure 7). Therefore, the antifouling sensor has excellent selectivity for the target ATP.

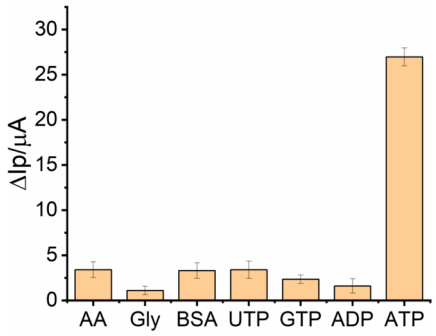

Figure 7. Response of electrochemical aptamer sensor to 1 nM AA, Gly, BSA, UTP, GTP, and ADP and 0.1 nM ATP. The error bar is the standard deviation of the results of three repeated measurements.

Subsequently, we further studied the reproducibility and repeatability of the antifouling electrochemical sensor. First, in order to assess reproducibility, the ATP of 10 pM was detected with five newly prepared sensors, and the relative standard deviation was calculated to be 1.86%, indicating that it had acceptable reproducibility. Then, its repeatability was studied with the same sensor, and after detecting the ATP of 10 pM five times, the relative standard deviation was calculated to be 1.69%. The stability of the sensor was evaluated by continuous CV scans; after 30 CV scans, the current signal remained stable as shown in Figure S5. In addition, the current signal of the sensor stored at 4 °C in the refrigerator for 1 week is 92.3% of the original signal, indicating that the sensor has good stability.

3.8. Detection of ATP in Human Serum Samples. In order to prove the practicability of the constructed antifouling sensor, we selected the serum as the sample, heated the serum extracted from the hospital at 45 °C for 10 min, centrifuged, diluted the supernatant 50 times, dropped it on the sensor, and incubated it for 1.5 h, detected the change of current signal before and after incubation by DPV method, and calculated the content of ATP in the serum according to the linear equation of peak current and ATP concentration. It can be seen from Table 2 that the sensor has a good recovery rate of ATP in serum samples; the recovery rate range is 99.5%−106%, and the relative standard deviation range is 0.4%−2.88%. Therefore, the results showed that the antifouling electrochemical sensor has good clinical application performance.

Table 2. Detection of ATP in the Blood Sample

sample	added (pM)	found (pM)	recovery (%)	RSD (%,n = 3)
Sample 1	10	10.31	103.3	2.88
Sample 2	1000	995	99.5	0.4
Sample 3	10000	10602	106	2.02

4. CONCLUSIONS

In summary, an antifouling electrochemical sensor was constructed based on the interpenetrating network of Y-DNA scaffold and conductive polyaniline hydrogel. Cellulose nanocrystals and polypeptides served as the antifouling material, and ATP aptamer was used as the cross-linker of a Y-type DNA network to increase the active sit except as an aptamer for ATP detection. High conductivity, porous structure, and good

https://doi.org/10.1021/acsami.2c10081
ACS Appl. Mater. Interfaces 2022, 14, 40624−40632

biocompatibility of polyaniline hydrogel have improved the detection sensitivity. The introduction of cellulose nanocrystals and polypeptides as antifouling materials in polyaniline hydrogel can prevent nonspecific adsorption in complex biological media. In conclusion, the hydrogels that we prepared integrated high conductivity, antifouling, and signal amplification performance. The detection results showed that the antifouling electrochemical biosensor has a wide linear range of 0.1 pM−1 μM and a low detection limit of 0.025 pM for ATP detection. It is expected to provide a certain reference value for the detection of other biological small molecules.

■ ASSOCIATED CONTENT

Supporting Information

The Supporting Information is available free of charge at https://pubs.acs.org/doi/10.1021/acsami.2c10081.

Figures of gelling mechanism of CPH−CNC hydrogel, infrared spectrogram of polyaniline hydrogel and its monomers, change of DPV signal of the sensor with or without aptamer in the presence of ATP, cyclic voltammetry curves of the composite conductive hydrogel at different scanning rates, and cyclic voltammetry curves of the antifouling sensor in the PB (0.2 M, pH = 7.4) solution and table of proposed antifouling electrochemical sensor compared with other methods for the detection of ATP (PDF)

■ AUTHOR INFORMATION

Corresponding Authors

Xiaoyan He − *Key Laboratory of Bioelectrochemistry and Environmental Analysis of Gansu, College of Chemistry and Chemical Engineering, Northwest Normal University, Lanzhou 730070, P. R. China;* orcid.org/0000-0002-4396-7903; Email: hexy09@163.com

Xiaoquan Lu − *Key Laboratory of Bioelectrochemistry and Environmental Analysis of Gansu, College of Chemistry and Chemical Engineering, Northwest Normal University, Lanzhou 730070, P. R. China;* orcid.org/0000-0003-2375-668X; Email: luxq@nwnu.edu.cn

Authors

Nan Sun − *Key Laboratory of Bioelectrochemistry and Environmental Analysis of Gansu, College of Chemistry and Chemical Engineering, Northwest Normal University, Lanzhou 730070, P. R. China*

Hui Jia − *Key Laboratory of Bioelectrochemistry and Environmental Analysis of Gansu, College of Chemistry and Chemical Engineering, Northwest Normal University, Lanzhou 730070, P. R. China*

Miaomiao Hou − *Key Laboratory of Bioelectrochemistry and Environmental Analysis of Gansu, College of Chemistry and Chemical Engineering, Northwest Normal University, Lanzhou 730070, P. R. China*

Zheping Tan − *Key Laboratory of Bioelectrochemistry and Environmental Analysis of Gansu, College of Chemistry and Chemical Engineering, Northwest Normal University, Lanzhou 730070, P. R. China*

Complete contact information is available at: https://pubs.acs.org/10.1021/acsami.2c10081

Author Contributions

All authors have given approval to the final version of the manuscript.

Notes

The authors declare no competing financial interest.

■ ACKNOWLEDGMENTS

This work was supported by the National Natural Science Foundation of China (NSFC) (No. 21765019) and the Funds for Creative Research Groups of Gansu Province (No. 21JR7RA160).

■ REFERENCES

(1) Meng, X. S.; Bai, H.; Ma, Q.; Zhang, P.; Ma, H.; Deng, Y. L. Broad Targeted Analysis of Neurochemicals in Rat Serum using Liquid Chromatography Tandem Mass Spectrometry with Chemical Derivatization. *J. Sep Sci.* **2020**, *43* (21), 4006−4017.

(2) Nishizawa, M.; Walinda, E.; Morimoto, D.; Kohn, B.; Scheler, U.; Shirakawa, M.; Sugase, K. Effects of Weak Nonspecific Interactions with ATP on Proteins. *J. Am. Chem. Soc.* **2021**, *143* (31), 11982−11993.

(3) Mishra, A.; Dhiman, S.; George, S. J. ATP-Driven Synthetic Supramolecular Assemblies: From ATP as a Template to Fuel. *Angew. Chem., Int. Ed.* **2021**, *60* (6), 2740−2756.

(4) Li, Z.; Xu, X.; Yu, F.; Fei, J.; Li, Q.; Dong, M.; Li, J. Oriented Nanoarchitectonics of Bacteriorhodopsin for Enhancing ATP Generation in a FoF1-ATPase-Based Assembly System. *Angew. Chem., Int. Ed.* **2022**, *61* (16), e202116220.

(5) Wu, L.; Qu, X. Cancer Biomarker Detection: Recent Achievements and Challenges. *Chem. Soc. Rev.* **2015**, *44* (10), 2963−2997.

(6) Li, F.; Hu, X.; Wang, F.; Zheng, B.; Du, J.; Xiao, D. A fluorescent "on-off-on" Probe for Sensitive Detection of ATP Based on ATP Displacing DNA from Nanoceria. *Talanta* **2018**, *179*, 285−291.

(7) Li, X.; Peng, Y.; Chai, Y.; Yuan, R.; Xiang, Y. A Target Responsive Aptamer Machine for Label-Free and Sensitive Non-Enzymatic Recycling Amplification Detection of ATP. *Chem. Commun.* **2016**, *52* (18), 3673−3676.

(8) Xie, H.; Chai, Y.; Yuan, Y.; Yuan, R. Highly Effective Molecule Converting Strategy Based on Enzyme-Free Dual Recycling Amplification for Ultrasensitive Electrochemical Detection of ATP. *Chem. Commun.* **2017**, *53* (59), 8368−8371.

(9) Huang, Z.; Yu, S.; Jian, M.; Weng, Z.; Deng, H.; Peng, H.; Chen, W. Ultrasensitive Glutathione-Mediated Facile Split-Type Electrochemiluminescence Nanoswitch Sensing Platform. *Anal. Chem.* **2022**, *94* (4), 2341−2347.

(10) Xue, X.; Wang, F.; Zhou, J.; Chen, F.; Li, Y.; Zhao, J. Online Cleanup of Accelerated Solvent Extractions for Determination of Adenosine 5′-Triphosphate (ATP), Adenosine 5′-Diphosphate (ADP), and Adenosine 5′-Monophosphate (AMP) in Royal Jelly using High-Performance Liquid Chromatography. *J. Agric. Food Chem.* **2009**, *57* (11), 4500−4505.

(11) Jender, M.; Novo, P.; Maehler, D.; Munchberg, U.; Janasek, D.; Freier, E. Multiplexed Online Monitoring of Microfluidic Free-Flow Electrophoresis via Mass Spectrometry. *Anal. Chem.* **2020**, *92* (9), 6764−6769.

(12) Wu, Z.; Liu, M.; Liu, Z.; Tian, Y. Real-Time Imaging and Simultaneous Quantification of Mitochondrial H_2O_2 and ATP in Neurons with a Single Two-Photon Fluorescence-Lifetime-Based Probe. *J. Am. Chem. Soc.* **2020**, *142* (16), 7532−7541.

(13) Fu, S.; Zhu, Y.; Zhang, Y.; Zhang, M.; Zhang, Y.; Qiao, L.; Yin, N.; Song, K.; Liu, M.; Wang, D. Recent Advances in Carbon Nanomaterials-Based Electrochemical Sensors for Phenolic Compounds Detection. *Microchem. J.* **2021**, *171*, 106776−106798.

(14) Yu, Z.; Gong, H.; Xu, J.; Li, Y.; Xue, F.; Zeng, Y.; Liu, X.; Tang, D. Liposome-Embedded $Cu_{2-x}Ag_xS$ Nanoparticle-Mediated Photothermal Immunoassay for Daily Monitoring of cTnI Protein Using a Portable Thermal Imager. *Anal. Chem.* **2022**, *94* (20), 7408−7416.

(15) Zeng, R.; Gong, H.; Li, Y.; Li, Y.; Lin, W.; Tang, D.; Knopp, D. CRISPR-Cas12a-Derived Photoelectrochemical Biosensor for Point-Of-Care Diagnosis of Nucleic Acid. *Anal. Chem.* **2022**, *94* (20), 7442−7448.
(16) Jiang, C.; Wang, G.; Hein, R.; Liu, N.; Luo, X.; Davis, J. J. Antifouling Strategies for Selective In Vitro and In Vivo Sensing. *Chem. Rev.* **2020**, *120* (8), 3852−3889.
(17) Patel, J.; Radhakrishnan, L.; Zhao, B.; Uppalapati, B.; Daniels, R. C.; Ward, K. R.; Collinson, M. M. Electrochemical Properties of Nanostructured Porous Gold Electrodes in Biofouling Solutions. *Anal. Chem.* **2013**, *85* (23), 11610−11618.
(18) Silva, T. A.; Khan, M. R. K.; Fatibello-Filho, O.; Collinson, M. M. Simultaneous Electrochemical Sensing of Ascorbic Acid and Uric Acid under Biofouling Conditions using Nanoporous Gold Electrodes. *J. Electroanal. Chem.* **2019**, *846*, 113160−113169.
(19) Hui, N.; Sun, X.; Niu, S.; Luo, X. PEGylated Polyaniline Nanofibers: Antifouling and Conducting Biomaterial for Electrochemical DNA Sensing. *ACS Appl. Mater. Interfaces* **2017**, *9* (3), 2914−2923.
(20) Qi, L.; Jiang, T.; Liang, R.; Qin, W. Enhancing the Oil-Fouling Resistance of Polymeric Membrane Ion-Selective Electrodes by Surface Modification of a Zwitterionic Polymer-Based Oleophobic Self-Cleaning Coating. *Anal. Chem.* **2021**, *93* (18), 6932−6937.
(21) Li, Y.; Han, R.; Chen, M.; Yang, X.; Zhan, Y.; Wang, L.; Luo, X. Electrochemical Biosensor with Enhanced Antifouling Capability Based on Amyloid-like Bovine Serum Albumin and a Conducting Polymer for Ultrasensitive Detection of Proteins in Human Serum. *Anal. Chem.* **2021**, *93* (42), 14351−14357.
(22) Yang, W.; Pan, M.; Zhang, J.; Zhang, L.; Lin, F.; Liu, X.; Huang, C.; Chen, X. Z.; Wang, J.; Yan, B.; Zeng, H. A Universal Strategy for Constructing Robust and Antifouling Cellulose Nanocrystal Coating. *Adv. Funct. Mater.* **2022**, *32* (8), 2109989−2110001.
(23) Wang, G.; Han, R.; Li, Q.; Han, Y.; Luo, X. Electrochemical Biosensors Capable of Detecting Biomarkers in Human Serum with Unique Long-Term Antifouling Abilities Based on Designed Multifunctional Peptides. *Anal. Chem.* **2020**, *92* (10), 7186−7193.
(24) Song, Z.; Chen, M.; Ding, C.; Luo, X. Designed Three-in-One Peptides with Anchoring, Antifouling, and Recognizing Capabilities for Highly Sensitive and Low-Fouling Electrochemical Sensing in Complex Biological Media. *Anal. Chem.* **2020**, *92* (8), 5795−5802.
(25) Zhang, X.; Huang, H.; Li, Q.; Yu, H.; Tian, X.; Zhao, M.; Zhang, H. Facile Dual-Functionalization of Polyamide Reverse Osmosis Membrane by a Natural Polypeptide to Improve the Antifouling and Chlorine-Resistant Properties. *J. Membr. Sci.* **2020**, *604*, 118044−118054.
(26) Bai, J.; Wang, R.; Ju, M.; Zhou, J.; Zhang, L.; Jiao, T. Facile Preparation and High Performance of Wearable Strain Sensors based on Ionically Cross-Linked Composite Hydrogels. *Sci. China Mater.* **2021**, *64* (4), 942−952.
(27) Zhang, C.; Wang, M.; Jiang, C.; Zhu, P.; Sun, B.; Gao, Q.; Gao, C.; Liu, R. Highly Adhesive and Self-Healing γ-PGA/PEDOT:PSS Conductive Hydrogels Enabled by Multiple Hydrogen Bonding for Wearable Electronics. *Nano Energy* **2022**, *95*, 106991−106999.
(28) Walker, B. W.; Lara, R. P.; Mogadam, E.; Yu, C. H.; Kimball, W.; Annabi, N. Rational Design of Microfabricated Electroconductive Hydrogels for Biomedical Applications. *Prog. Polym. Sci.* **2019**, *92*, 135−157.
(29) Li, L.; Zhang, Y.; Lu, H.; Wang, Y.; Xu, J.; Zhu, J.; Zhang, C.; Liu, T. Cryopolymerization Enables Anisotropic Polyaniline Hybrid Hydrogels with Superelasticity and Highly Deformation-Tolerant Electrochemical Energy Storage. *Nat. Commun.* **2020**, *11* (1), 62.
(30) Moussa, M.; El-Kady, M. F.; Dubal, D.; Tung, T. T.; Nine, M. J.; Mohamed, N.; Kaner, R. B.; Losic, D. Self-Assembly and Cross-Linking of Conducting Polymers into 3D Hydrogel Electrodes for Supercapacitor Applications. *ACS Appl. Energy Mater.* **2020**, *3* (1), 923−932.
(31) Cao, T.; Jia, H.; Dong, Y.; Gui, S.; Liu, D. In Situ Formation of Covalent Second Network in a DNA Supramolecular Hydrogel and Its Application for 3D Cell Imaging. *ACS Appl. Mater. Interfaces* **2020**, *12* (4), 4185−4192.
(32) Wei, Y.; Wang, K.; Luo, S.; Li, F.; Zuo, X.; Fan, C.; Li, Q. Programmable DNA Hydrogels as Artificial Extracellular Matrix. *Small* **2022**, 2107640−210753.
(33) Mo, F.; Jiang, K.; Zhao, D.; Wang, Y.; Song, J.; Tan, W. DNA Hydrogel-Based Gene Editing and Drug Delivery Systems. *Adv. Drug Deliv Rev.* **2021**, *168*, 79−98.
(34) Li, W.; Gao, F. X.; Wang, X. Q.; Zhang, N.; Ma, M. Strong and Robust Polyaniline-Based Supramolecular Hydrogels for Flexible Supercapacitors. *Angew. Chem., Int. Ed.* **2016**, *55*, 9196−9201.
(35) Li, Y.; Han, R.; Chen, M.; Zhang, L.; Wang, G.; Luo, X. Bovine Serum Albumin-Cross-Linked Polyaniline Nanowires for Ultralow Fouling and Highly Sensitive Electrochemical Protein Quantification in Human Serum Samples. *Anal. Chem.* **2021**, *93* (9), 4326−4333.
(36) Liang, X.; Pei, X.; Yang, Y.; Jia, E.; Zhou, H.; Xiang, S.; Lin, F.; Tan, Y. A Robust PVA/C/Sponge Composite Hydrogel with Improved Photothermal Interfacial Evaporation Rate Inspired by the Chimney Effect. *Desalination* **2022**, *531*, 115720−115728.
(37) Wang, X.; Gao, F.; Gong, Y.; Liu, G.; Zhang, Y.; Ding, C. Electrochemical Aptasensor Based on Conductive Supramolecular Polymer Hydrogels for Thrombin Detection with High Selectivity. *Talanta* **2019**, *205*, 120140−120145.
(38) Liu, X.; He, X.; Yang, B.; Lai, L.; Chen, N.; Hu, J.; Lu, Q. Dual Physically Cross-Linked Hydrogels Incorporating Hydrophobic Interactions with Promising Repairability and Ultrahigh Elongation. *Adv. Funct. Mater.* **2021**, *31* (3), 2008187−2008195.

https://doi.org/10.1021/acsami.2c10081
ACS Appl. Mater. Interfaces 2022, 14, 40624−40632